Metallophysics and Advanced Technologies
Металофіз. новітні технол.
Metallofiz. Noveishie Tekhnol.
2023, vol. 45, No. 10, pp. 1165–1177
https://doi.org/10.15407/mfint.45.10.1165
Reprints available directly from the publisher

PACS numbers: 61.05.cp, 77.84.Bw, 78.30.Hv, 81.05.Je, 81.20.Ev, 81.20.Wk, 82.80.Pv

Single-Step Pressureless Synthesis of the High-Purity Ti_3AlC_2 MAX-Phase by Fast Heating

I. M. Kirian, A. M. Lakhnik, O. Yu. Khyzhun*, I. V. Zagorulko, A. S. Nikolenko**, and O. D. Rud'

G. V. Kurdyumov Institute for Metal Physics, N.A.S. of Ukraine,
36 Academician Vernadsky Blvd.,
UA-03142 Kyiv, Ukraine
**I. M. Frantsevych Institute for Problems in Materials Science, N.A.S. of Ukraine,*
3 Omeljan Pritsak Str.,
UA-03142 Kyiv, Ukraine
***V. E. Lashkaryov Institute of Semiconductor Physics, N.A.S. of Ukraine,*
41 Nauky Ave.,
UA-03028 Kyiv, Ukraine

A simple approach is presented to synthesise the high-purity MAX phase by the pressureless method. This method is featured by the short time in duration. The process is executed with a high heating rate (up to $\cong 10^2$ K/min) that inhibits the formation of the objectionable phases and limits elemental loss due to the short-time process. The samples containing $\cong 96\%$ wt. of the MAX phase Ti_3AlC_2 are successfully synthesised using the proposed technique.

Key words: MAX phase, pressureless synthesis, fast heating, ball milling.

Представлено простий підхід щодо синтези MAX-фази високої чистоти методом швидкісного нагріву без застосування тиску під час спікання. Процес здійснюється за високої швидкости нагрівання (до $\cong 10^2$ К/хв.), що перешкоджає утворенню небажаних фаз і обмежує втрати елементів завдяки короткій тривалості процесу. За запропонованою методикою синтезовано зразки, що містять $\cong 96\%$ ваг. MAX-фази Ti_3AlC_2.

Ключові слова: MAX-фаза, безконтактна синтеза (без тиску), швидкий нагрів, кульове розмелювання.

Corresponding author: Oleksandr Dmytrovych Rud'
E-mail: rud@imp.kiev.ua

Citation: I. M. Kirian, A. M. Lakhnik, O. Yu. Khyzhun, I. V. Zagorulko, A. S. Nikolenko, and O. D. Rud', Single-Step Pressureless Synthesis of the High-Purity Ti_3AlC_2 MAX-Phase by Fast Heating, *Metallofiz. Noveishie Tekhnol.*, **45**, No. 10: 1165–1177 (2023). DOI: 10.15407/mfint.45.10.1165

(Received 3 July, 2023; in final version, 19 September, 2023)

1. INTRODUCTION

Materials featured by an unusual combination of physical and mechanical properties always attract particular attention. Such class of materials include recently discovered layered ternary nitrides/carbides—MAX phases, which are described by the generally accepted formula $M_{n+1}AX_n$ ($n = 1$, 2 and 3), where M is a transition metal, A is the elements of the A-subgroup of the Mendeleev table and X is C or N [1–3] and having a crystalline hexagonal structure with a space group $P6_3/mmc$ [4]. The MAX phases integrate the properties of both metals and ceramics. They are characterized by low density, high thermal and electrical conductivity, high strength, low elastic modulus, high corrosion resistance, high melting point, resistance to oxidation and heat shock. So, unusual combination of properties in MAX phases is summoned by its crystal lattice structure, which can be described as a set of alternated planes formed by M and A atoms. The carbon (or nitrogen) atoms in this crystal lattice occupy the octahedral pores formed by the M atoms [4]. Among the wide variety of MAX phases, the particular interest of researchers is attracted to the titanium based MAX phases Ti_2AlC Ti_2AlN, Ti_3AlC_2 and Ti_3SiC_2. The MAX phases Ti–Si–C are the most studied. Unfortunately, the Ti–Al–C(N) MAX phases have been investigated notably less. The MAX phases of Ti_3SiC_2, Ti_3AlC_2 and Ti_4AlN_3 have higher mechanical properties than α-Ti, β-Ti and Mo but are inferior then titanium carbide TiC [5]. The Ti_3AlC_2 phase has better mechanical characteristics than Ti_2AlC phase [6]. The MAX phase Ti_3AlC_2 is a promising material for widespread industrial application. Several different synthesis methods are applied to fabricate MAX phases. Pressureless sintering is the simplest way to synthesize the MAX phases [7]. Mechanical alloying is another convenient and effective method of producing MAX phase powders [8]. However, the mechanically milled Ti–Al–C elemental powder mixtures yield enough small fraction of the MAX phase. The self-propagating high-temperature synthesis (SHS) is the most promising method. Unlike other energy-intensive and time-durable methods, the SHS process occurs within a few seconds. However, under the SHS sintering, in addition to the MAX phase, other ones always additionally formed. These phases significantly degrade the properties of the sintered compact [9]. For example, under the synthesis process of the Ti_3AlC_2 MAX phase, the titanium carbide TiC and the Al_3Ti, TiAl and Ti_3Al intermetallics can be formed. The hot isostatic pressing method (HIP) also enables the manufacture of almost pure MAX phases [10]. However, it is a complicated technological process, which increases the expenses of the fabri-

cated material. The hot pressing method is technologically more straightforward than the HIP one [11, 12]. The spark plasma sintering method is also widely involved in the synthesis of MAX phases [12–14].

There is one essential complexion that should be noted: the synthesis temperature of the MAX phase (1300–1500°C [15]) is remarkably higher than the aluminium melting temperature (660°C). Therefore, partial evaporation of aluminium happens during the heating of the powder mixture to the synthesis temperature. It results in a significant stoichiometric ratio violation of the elements in the sintered compact in contrast to the initial powder mixture. This is a crucial challenge in the synthesis of the Ti_3AlC_2 MAX phase.

There are several ways to overcome this drawback. The first and easiest way is an expanding of the aluminium percentage in the initial powder blend. Another way is the employ of fusible dopants to inhibit the aluminium evaporation and prevent thermal explosion between components under the sintering process. It has been proposed to use boron oxide (B_2O_3) and Sn as low-temperature additives [16, 17]. The authors of these works claim that the addition of B_2O_3 and Sn prevents a thermal explosive reaction in a mixture of elemental Ti, Al, and carbon powders and, thereby, contributes to the synthesis of the MAX phase of Ti_3AlC_2 high purity. However, the impact of these dopants on the synthesis process of MAX phases and their structural state was not cleared in detail yet.

In this paper, we focused on the study of the action of the boron oxide B_2O_3 and heating rates on the structural and phase state and electronic structure of the MAX phase Ti_3AlC_2.

2. MATERIALS AND METHODS

Two powder blends were prepared for investigation. In the first case, the elemental powders of Ti, Al, and spectrally pure graphite were mixed in an atomic ratio of 3:1.1:2. Since the partial loss of aluminium occurs due to its evaporation at high temperatures, the aluminium proportion in this sample was taken more than a stoichiometric value—1.1 instead 1. The second sample (in addition to Ti, Al and C mixed in a same ratio of 3:1.1:2, also) additionally contained with 5% wt. boron oxide (B_2O_3) as additive. The powder mixture homogenization was performed on a high-energy laboratory planetary mill (Fritsch Pulverisette P-6) at room temperature for 1 hour. The rotational speed of the grinding container was 200 rpm, and the balls-to-powder mass ratio was 20:1. Homogenized powder blends were compacted as cylindrical pellets of 14 mm in diameter at a pressure of $\cong$ 200 MPa. Then, compressed pellets were sintered at different temperatures and heating rates in an argon atmosphere.

X-ray diffraction patterns were recorded using a powder diffrac-

tometer (HZG-4) in the Bragg–Brentano geometry with radiation CoK_α. The XRD patterns were processed by the Rietveld refinement technique using the MAUD software [18]. Raman scattering experiments were performed at room temperature in backscattering geometry using a T-64000 Horiba Jobin-Yvon spectrometer equipped with a thermo-electrically cooled CCD detector and an Olympus BX41 confocal microscope. The Raman spectra were excited with by cyan line of the Ar–Kr laser (wavelength $\lambda = 488$ nm). The laser beam was focused on the sample surface through the ×50/NA 0.75 lens in a spot $\cong 1$ μm. The laser radiation power at the sample surface was in the range of 2.5–10 mW. The XPS spectra were acquired with the UHV-Analysis-System (SPECS Surface Nano Analysis Company, Berlin, Germany) supplied with a hemispherical PHOIBOS 150 analyser. The XPS spectra were excited by the MgK_α source of x-ray radiation ($h\nu = 1253.6$ eV) and were recorded at a residual pressure of about $5 \cdot 10^{-8}$ Pa in an ion-pumped chamber of the UHV-Analysis-System. The measurements were executed at constant pass energy of 30 eV. The present XPS measurements were performed with the use of a flood gun supplied with the UHV-Analysis-System. To remove hydrocarbons and oxygen-contained species adsorbed on the sample surface due to its contact with laboratory air, we treated the sample under study with 3 kV Ar^+ ions (6 min duration, 16 mA/cm^2 ion current density). DSC curves were recorded using a Netzsch 404 F1 Pegasus® calorimeter in the temperature range from 25 to 1500°C at a heating/cooling rate of 40 K/min under a dynamic high-purity helium flow. Yttrium oxide Y_2O_3 crucibles were used. Estimation of critical temperatures was done with Netzsch Proteus Thermal Analysis software.

3. RESULTS AND DISCUSSION

Figure 1 shows DSC thermograms for the powder blends $Ti_3Al_{1.1}C_2$ and $Ti_3Al_{1.1}C_2 + 5\%$ wt. B_2O_3 after homogenization in a ball mill for 1 hour. The endothermic peaks formed at temperatures around 662.5 and 656.3°C in both DSC curves correspond to the melting of Al.

Further temperature increase facilitates active interaction between titanium and aluminium. This process is issued by the formation of the Ti_3Al intermetallic. Two exothermic peaks are observed on the DSC curves at 728.4 (Fig. 1, *a*) and 760.5°C (Fig. 1, *b*), respectively. These peaks are attributed to the Al_3Ti phase formation [19]. Thus the DSC curves (Fig. 1) clearly shows the formation temperature of the Ti_3Al intermetallic in the sample containing boron oxide is shifted towards higher values. On the DSC curve of the $Ti_3Al_{1.1}C_2$ mixture at 929.1°C, a weak exothermic peak is observed (Fig. 1, *a*). It indicates the formation of the TiC phase according to the literature [20].

In contrary, on the DSC curve of the mixture $Ti_3Al_{1.1}C_2 + 5\%$ wt.

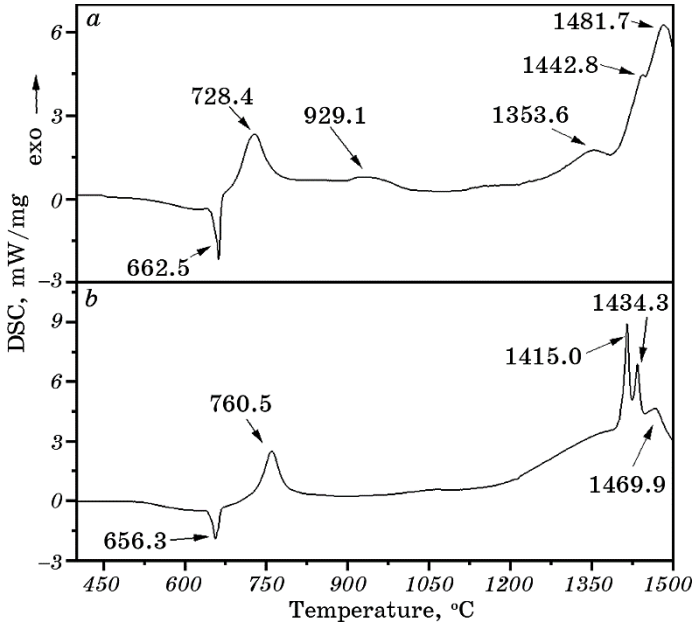

Fig. 1. DSC for the as-prepared powder blends homogenized: $Ti_3Al_{1.1}C_2$ (*a*), $Ti_3Al_{1.1}C_2$ + 5% wt. B_2O_3 (*b*).

B_2O_3, the peak at this temperature typical of TiC is not observed (Fig. 1, *b*). In addition, there are exothermic peaks on the DSC curves for both samples in the temperature ranges of ≅ 1350–1485°C and ≅ 1400–1475°C, respectively.

Further, the research was focused on determining the nature of the origin of the maxima on the DSC curves in the range of the indicated temperatures. The simple sintering method was used to obtain composites at these temperatures. Pressed pellets were heated to the indicated temperatures at a rate of 40 K/min and quickly cooled down to room temperature. XRD patterns for the powder mixture $Ti_3Al_{1.1}C_2$ sintered at the temperatures1353°C, 1442°C, and 1481°C are shown in Fig. 2.

Obviously, the $Ti_3Al_{1.1}C_2$ mixture sintered at a temperature of 1353°C contains several phases (Fig. 2, *a*). The most intense peaks on the XRD pattern belong to the titanium carbide (TiC), Ti_3AlC phase, and Ti_2AlC MAX phase, respectively. The percentage of the TiC, Ti_3AlC and Ti_2AlC in the sample estimated by full-profile analysis is about ≅ 35, ≅ 11, and ≅ 24% wt., respectively. Moreover, there are peaks related to graphite and titanium are in the XRD pattern (Fig. 2, *a*), as well. Thus, the reaction is not fully completed at 1353°C between Ti, Al, and graphite. The amount of unreacted graphite and titanium in the sample are ≅ 23 and ≅ 7% wt., respectively. When the temperature rises to 1442°C, the peaks related to titanium and graphite on the

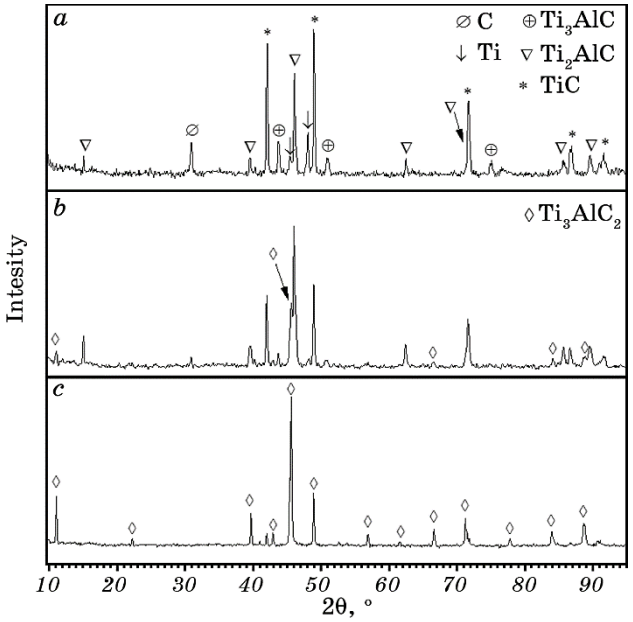

Fig. 2. XRD patterns of the sample synthesized by sintering of the $Ti_3Al_{1.1}C_2$ powder mixture for 1353°C (*a*), 1442°C (*b*), 1481°C (*c*) at the heating rate of 40 K/min.

XRD pattern entirely disappear (Fig. 2, *b*).

However, along with other phases, peaks related to the Ti_3AlC_2 MAX phase appear on the x-ray diffraction pattern. The content of this phase in the sintered sample is ≅ 27% wt. There are graphite ≅ 6% wt., TiC ≅ 22% wt., Ti_2AlC ≅ 41% wt. and Ti_3AlC ≅ 4% wt. in this sample, too. When the sample is heated to 1481°C, mainly Ti_3AlC_2 MAX phase is formed (≅ 96% wt.) (Fig. 2, *c*). The rest ≅ 4% wt. is the undesired TiC impure phase. The lattice parameters values for MAX phase Ti_3AlC_2 and TiC, acquired from the XRD full-profile refinement, are $a = 0.3072$ nm, $b = 1.8560$ nm, and $a = 0.3060$ nm, $b = 1.4855$ nm, respectively.

Three peaks are clearly distinguished on the DSC thermogram for $Ti_3Al_{1.1}C_2 + 5\%$ wt. B_2O_3 blend at temperatures 1415, 1430 and 1470°C, respectively. As for the previous sample, heating was performed at a rate of 40 K/min to the indicated temperatures, followed by cooling. The XRD patterns of the sintered samples are shown in Fig. 3.

There is a marked distinction in the phase formation in the sample containing boron oxide from the previous one. As follows from the full-profile refinement of the XRD diffraction pattern, there are only two phases in the sintered sample at 1415°C—TiC and Ti_3AlC_2 (Fig. 3, *a*). The most intensive peaks are related to TiC. Titanium carbide TiC dominates in this sample at ≅ 90% wt. The percentage of the MAX phase in the sample is low ≅ 10% wt.

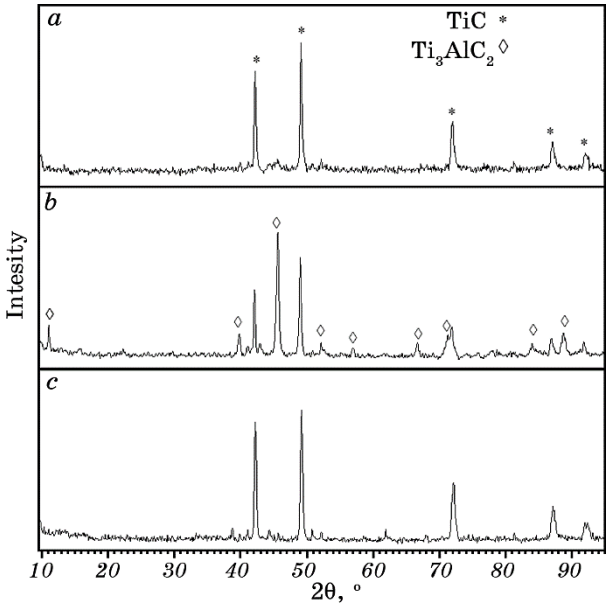

Fig. 3. XRD patterns of the $Ti_3Al_{1.1}C_2 + 5\%$ wt. B_2O_3 powder blend sintered at 1415°C (*a*), 1435°C (*b*), 1470°C (*c*), respectively, at the heating rate of 40 K/min.

The peak intensity ratio for TiC and the MAX phase (Fig. 3, *b*) changes noticeably on the XRD pattern. The intensity of the peaks related to the MAX phase rises. On the contrary, the intensity of the peaks associated with the TiC decreases. It evidences the percentage of the TiC and MAX phase is altered in the sample after heating to a temperature of 1435°C. There are ≅ 70% wt. of the MAX phase Ti_3AlC_2 and ≅ 30% wt. of the TiC in this sample (Fig. 3, *b*). The lattice parameters for both Ti_3AlC_2 and TiC phases are $a = 0.3075$ nm, $b = 1.8571$ nm, and $a = 0.3051$ nm, $b = 1.4983$ nm, respectively.

A further temperature sintering increase up to 1470°C causes a significant change in the phase composition of the sample. The titanium carbide TiC prevails in the sintered sample at the temperature of 1470°C (Fig. 3, *c*) again. It has seen sharp reflexes related to TiC, but the peaks of the Ti_3AlC_2 phase almost disappear on the XRD. The percentage of Ti_3AlC_2 and TiC phases are ≅ 3% wt. and ≅ 97% wt., respectively.

It has been pointed out above, the maximum around the 1435°C on the DSC thermogram for the $Ti_3Al_{1.1}C_2 + 5\%$ wt. B_2O_3 sample is caused by the Ti_3AlC_2 MAX phase formation (see Fig. 3, *b*). However, the MAX phase amount in the sample heated at a rate of 40 K/min is not above 70% wt. To elucidate the influence of the heating rate on the formation of the MAX phase, the four samples were sintered during heating to 1435°C with rates of 40, 100, 120, and 150 K/min, respec-

tively (Fig. 4). The amount of the Ti_3AlC_2 phase in the sample heated at a rate of 100 K/min is increased up to ≅ 88% wt. Around 12% wt., the TiC is in this sample too (Fig. 4, *b*).

Future increasing the heating rate up to 120 K/min changes the phase composition of the sample. As a result, the synthesized sample contains ≅ 94% wt. of the MAX phase Ti_3AlC_2 and ≅ 6% wt. of the TiC phase (Fig. 4, *c*). The lattice parameters for Ti_3AlC_2 and TiC acquired by full-profile XRD refinement are $a = 0.3074$ nm, $b = 1.8575$ nm, and $a = 0.3059$ nm, $b = 1.490$ nm, respectively. Thus, fast heating of the $Ti_3Al_{1.1}C_2 + 5\%$ wt. B_2O_3 blend provides a more yield of the Ti_3AlC_2 MAX phase in the sintered sample within a short time in contrast to lower heating rates. It needs more time to synthesize the same amount of the MAX phase in the sintered sample from the boron oxide B_2O_3-free $Ti_3Al_{1.1}C_2$ blend.

For the sample sintered at a heating rate of 150 K/min, a significant reduction in the content of the MAX phase in the composite to 85% wt. is observed (Fig. 4, *d*). At the same time, the content of the TiC phase increases to ≅ 15% wt.

The Raman spectra were recorded for the sample sintered under the heating of the $Ti_3Al_{1.1}C_2 + 5\%$ wt. B_2O_3 powder blend to the temperature of 1435°C at the rate of 120 K/min (Fig. 5). The Raman spectra

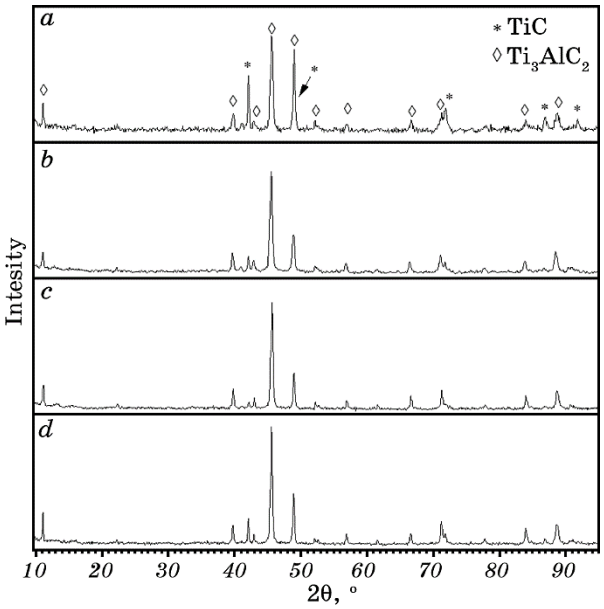

Fig. 4. XRD diffraction patterns for the $Ti_3Al_{1.1}C_2 + 5\%$ wt. B_2O_3 powder blend sintered at 1435°C at the heating rates: 40 K/min (*a*), 100 K/min (*b*), 120 K/min (*c*), 150 K/min (*d*).

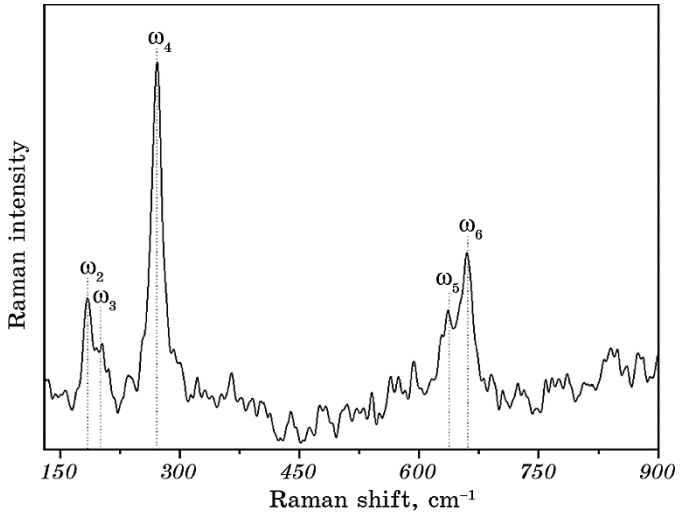

Fig. 5. Raman spectra of the MAX phase Ti_3AlC_2.

were registered in the various locations on the sample surface in the range of 150–900 cm^{-1}. The bands with frequencies of ≅ 183, 201, 270, 632 and 663 cm^{-1} specified to the Ti_3AlC_2 MAX phase are clearly distinguished on the spectra. These bands are symbolised as ω_2–ω_6 (Fig. 5) as in the papers [21, 22]. However, there are no bands in the Raman spectrum, which could be featured to boron oxide and titanium carbide.

To test elemental presence, peculiarities of the chemical bonding and energy distribution of the valence electronic states in MAX phase [23] synthesized by simple sintering (Ti_3AlC_2 + 5% wt. B_2O_3) mixture used x-ray photoelectron spectroscopy (XPS). Before studying, the sample surface was treated with Ar^+ ions. In many cases, such a surface treatment provides nearly complete removal of hydrocarbons and oxygen-contained species adsorbed on the sample surface. Figure 6 shows XPS core-level Ti 2*p*, Al 2*p*, C 1*s*, and O 1*s* spectra of the Ar^+ ion-irradiated surface of the Ti_3AlC_2. The background was approximated by Shirley's function and subtracted from the XPS spectra.

The binding energy values computed by the asymmetric Gaussian–Lorentzian fitting of XPS spectra for the core-level Ti 2*p*, Al 2*p*, C 1*s*, and O 1*s* states are summarized in Table 1.

The XPS core-level Ti 2*p* spectra consist of three components with binding energy located at about 454.8, 458.7, and 464.2 eV (Fig. 6, *a*), respectively. The Ti $2p_{3/2}$ core-level electrons yield binding energy at about 454.8 eV. This value is close to the binding energies of those electrons in TiC [23]. However, the Ti 2*p* spectrum of the surface also features Ti $2p_{3/2}$ (458.7 eV) and Ti $2p_{1/2}$ (464.2 eV) core-level peaks associat-

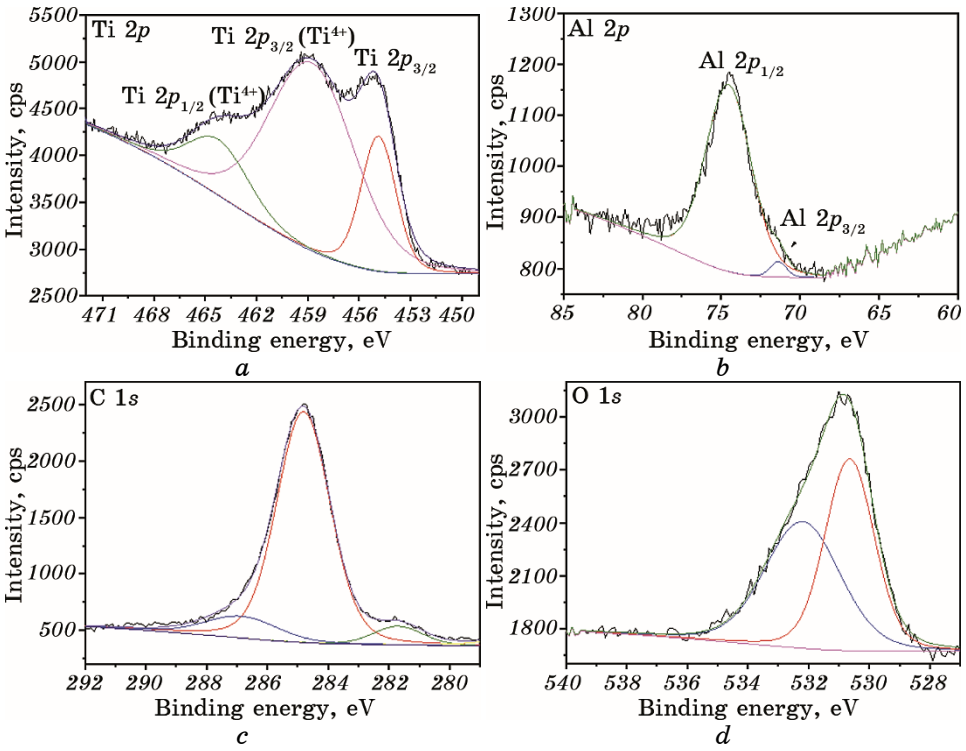

Fig. 6. XPS core-level Ti 2*p* (*a*), Al 2*p* (*b*), C 1*s* (*c*), O 1*s* (*d*) spectra of the Ti_3AlC_2 MAX phase radiated by 3 kV Ar^+ ion beam.

ed with Ti^{4+} due to surface oxidation by TiO_2 [24]. The XPS Al 2*p* spectra are presented in (Fig. 6, *b*). The spectrum of the surface is characterized by the existence of two $2p_{3/2}$ and $2p_{1/2}$ spin–orbit splits. The first component (74.5 eV) corresponds to aluminium in Al_2O_3, while the binding energy of the second one (71.9 eV) is close to that of metallic Al [23].

Figure 6, *c* presents the C 1*s* XPS spectrum of MAX phase Ti_3AlC_2 consisting of three components. The peak of the spectrum with its binding energy position at about 281.6 eV corresponds to carbon forming the C–Ti (Al) bonds. Its binding energy is close to that of carbon forming C–Ti bonds in titanium carbide TiC [23]. Other two peaks correspond to non-carbide components $C–C + CH_2$ at about 285.1 eV and C–OH ≅ 286.7 eV [25]. The O 1*s* XPS spectrum has asymmetric form (Fig. 6, *d*). It was fit by two components corresponding to TiO_2 and Al_2O_3 located at position 530.6 and 532.3 eV, respectively.

The B 1*s* XPS spectra of the pristine and Ar^+ ion-irradiated surfaces of MAX phase Ti_3AlC_2 are represented in Fig. 7.

The spectrum for the untreated surface has a maximum centred at ≅ 192.1 eV (Fig. 7, *a*). This binding energy corresponds to that of boron

TABLE 1. The binding energy values for the core-level Ti 2*p*, Al 2*p*, C 1*s*, O 1*s* states of the Ti_3AlC_2.

MAX phase	Components	Ti		Al		C	O
		$2p_{1/2}$, eV	$2p_{3/2}$, eV	$2p_{1/2}$, eV	$2p_{3/2}$, eV	1*s*, eV	1*s*, eV
Ti_3AlC_2	Ti–C		454.8			281.6	
	TiO_2	464.2	458.7				530.6
	Al_2O_3			74.5			532.3
	Al				71.9		
	C–C + CH_2					285.1	
	C–OH					286.7	

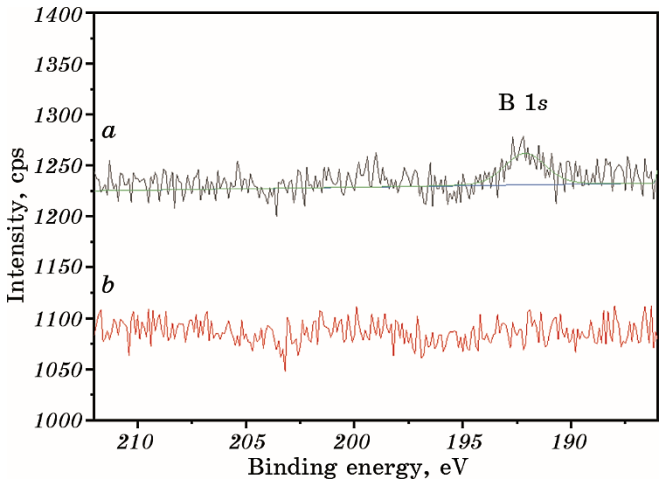

Fig. 7. XPS core-level B 1*s* spectra of the studied Ti_3AlC_2 MAX phase: pristine surface (*a*), irradiated with 3 kV Ar^+ ions (*b*).

atoms in B_2O_3 [23]. However, a surface treatment by Ar^+ ions causes the complete etching of boron atoms from the topmost surface layers (Fig. 7, *b*). So, boron oxide avoids both challenges: the Al evaporative loss and the thermal explosion simultaneously and does not remain as impurities in the produced Ti_3AlC_2 phase.

It should be noted two main results. First of all, it follows from the data presented above the fast heating rate enables completely inhibits the formation or minimizes the amount of titanium carbide, which is formed at a lower temperature than the MAX phase one in the Ti–Al–C system. The narrow domain for the Ti_3AlC_2 phase in the Ti–Al–C phase diagram [26] can be quickly reached by applying this way. Secondly, the boron oxide low melted dopant has been a crucial effect on the phase formation in the Ti–Al–C system. The boron oxide is uniformly

distributed over the surface of Ti, Al and graphite particles during the mechanical homogenizing of the powders. Due to the low melting temperature, boron oxide forms a liquid coat on the powders' particle surface at temperatures lower than the Al melting point. This liquid boron oxide dissolved aluminium oxide on the Al particle surface and promoted the solid-state reaction between aluminium and titanium even at relatively low temperatures. It obviously follows from the data presented for the boron oxide doped sample. Moreover, the low-melting boron oxide facilitates to overcome of both challenges as the aluminium loss due to vaporization and the thermal explosion caused by the reaction. The beneficial impact of the low-melting dopants as B_2O_3, Si and Sn was pointed out by many authors [17, 27–29].

Conventionally, various hot-pressing methods are applied to fabricate low-pored compacts. However, the MAX phases are not used entirely as solid porousless densified compacts, but as powder, too. The ternary carbides are widely used likewise as a reinforced component to fabricate metal-matrix composites with improved mechanical properties [30]. The pressureless fast heating/cooling method without durable exposure at high-temperature enables the fabrication of the MAX phase over a short time. The proposed approach could be adopted for systems, where target-sintering needs to achieve mainly single-phase materials and porosity is not crucial.

4. CONCLUSION

The MAX-phase of Ti_3AlC_2 was synthesized for the first time by fast heating sintering method.

It has investigated the impact of temperature, heating rate, and chemical composition of the initial powder blends on the phase formation under the sintering. It was found that mainly monophase sample ($\cong$ 96% wt. of the Ti_3AlC_2 and $\cong$ 4% wt. TiC) is formed from the $Ti_3Al_{1.1}C_2$ powder blend sintered by continuous heating at the rate of 40 K/min to the temperature of 1481°C.

The impact of the low melting additive (boron oxide) on the MAX phase synthesis under sintering has been investigated. However, at a heating rate of 40 K/min to the specified temperature, the maximum output of the Ti_3AlC_2 phase in the synthesized material is only 70% wt.; the remaining 30% wt. is TiC. Heating the mixture ($Ti_3Al_{1.1}C_2$ + 5% wt. B_2O_3) at a rate of 120 K/min to 1435°C results in an increase in the content of the MAX phase in the sample to $\cong$ 96% wt.

It is shown that, by varying the powder mixture chemical composition and the heating rate, it is possible to synthesize predominantly single-phase Ti_3AlC_2 carbide in a short time with minimum expenses.

This work was partially supported by the project No. 056/23 of the G. V. Kurdyumov Institute for Metal Physics, N.A.S. of Ukraine.

REFERENCES

1. M. Naguib, M. Kurtoglu, V. Presser, J. Lu, J. Niu, M. Heon, L. Hultman, Y. Gogotsi, and M. W. Barsoum, *Adv. Mater.*, **23**: 4248 (2011).
2. M. Sokol, V. Natu, S. Kota, and M. W. Barsoum, *Trends. Chem.*, **1**: 210 (2019).
3. C. Anirudh, A. V. Vaibhav Koushik, and U. N. Kempaiah, *Int. J. Emerging Technol. Adv. Eng.*, **4**, Iss. 8: 624 (2014).
4. I. M. Low, *Advances in Science and Technology of $M_{n+1}AX_n$ Phases* (Elsevier: 2012).
5. A. A. Smetkin and Iu. K. Maiorova, *Bulletin PNRPU Mech. Eng., Mater. Sci.*, **17**: 120 (2015) (in Russian).
6. X. H. Wang and Y. C. Zhou, *J. Mater. Sci. Technol.*, **26**: 385 (2010).
7. C. Peng, C.-A. Wang, Y. Song, and Y. Huang, *Mater. Sci. Eng. A*, **428**: 54 (2006).
8. J. F. Li, T. Matsuki, and R. Watanabe, *J. Am. Ceram. Soc.*, **85**, Iss. 4: 1004 (2004).
9. A. G. Zhou, C. A. Wang, Z. B. Ge, and L. Wu, *J. Mater. Sci. Lett.*, **20**: 1971 (2001).
10. T. El-Raghy and M. W. Barsoum, *J. Am. Ceram. Soc.*, **82**, Iss. 10: 2849 (2004).
11. C. Yanga, S. Z. Jin, B. Y. Liang, and S. S. Jia, *J. European Ceram. Soc.*, **29**: 181 (2009).
12. W. B. Zhou, B. C. Mei, J. Q. Zhu, and X. L. Hong, *Mater. Lett.*, **59**: 131 (2005).
13. O. Syzonenko, M. Prystash, A. Zaichenko, A. Torpakov, Ye. Lypian, A. Rud, I. Kirian, A. Lakhnik, E. Shregii, S. Prokhorenko, R. Wojnarowska-Nowak, and J. Kandrotaite, *Machines. Technologies. Materials*, **12**: 395 (2018).
14. A. D. Rud, A. M. Lakhnik, I. M. Kirian, O. N. Sizonenko, A. D. Zaychenko, N. S. Pristash, and N. D. Rud, *Mater. Today: Proc.*, **5**: 26084 (2018).
15. T. Ai, F. Wang, Y. Zhang, P. Jiang, and X. Yuan, *Adv. Appl. Ceram.*, **112**: 424 (2013).
16. C. Peng, C. Wang, and Y. Huang, *Key Eng. Mater.*, **280–283**: 1369 (2005).
17. A. Mingxing, Z. Hongxiang, Z. Yang, T. Zhaoyun, H. Zhenying, Z. Zhili, and L. Shibo, *J. Am. Ceram. Soc.*, **89**, Iss. 3: 1114 (2006).
18. L. Luterotti and S. Gialanella, *Acta Mater.*, **46**, Iss. 1: 101 (1998).
19. G. Zhang, J. Niu, and H. Xu, *J. Phys.: Conf. Ser.*, **1507**: 042007 (2020).
20. Y. Ma, T. Chen, L. Gou, and W. Ding, *Mater.*, **14**: 6739 (2021).
21. V. Presser, M. Naguib, L. Chaput, A. Togo, G. Hug, and M. W. Barsoum, *J. Raman Spectrosc.*, **43**: 168 (2012).
22. M. W. Barsoum, *MAX Phases: Properties of Machinable Ternary Carbides and Nitrides* (Weinheim: Wiley-VCH Verlag: 2013).
23. C. D. Wagner, W. M. Riggs, L. E. Davis, J. F. Moulder, and G. E. Muilenberg, *Handbook of X-Ray Photoelectron Spectroscopy* (Perkin-Elmer Corp.: 1979).
24. J. Halim, K. M. Cook, M. Naguib, P. Eklund, Y. Gogotsi, J. Rosenand, and M. W. Barsoum, *Appl. Surf. Sci.*, **362**: 406 (2016).
25. L. A. Näslund, O. E. Persson Per, and J. Rosen, *J. Phys. Chem. C*, **124**: 27732 (2020).
26. D. Bandyopadhyay, R. C. Sharma, and N. Chakraborti, *J. Phase Equilibria*, **21**: 195 (2000).
27. W. Zhou, B. Mei, J. Zhu, and X. Hong, *J. Mater. Sci.*, **40**: 2099 (2005).
28. S. Li, W. Xiang, H. Zhai, Y. Zhou, C. Li, and Z. Zhang, *Mater. Res. Bull.*, **43**: 2092 (2008).
29. Z. Y. Zhong, H. Saka, T. H. Kim, E. A. Holm, Y. F. Han, and X. S. Xie, *Mater. Sci. Forum*, **475–479**: 1247 (2005).
30. D. Zhao, S. Xia, Y. Wang, and M. Wang, *Appl. Phys. A*, **126**: 69 (2020).